USC–SIPI REPORT #343

Theory of Partially Adaptive Radar

by

J. Scott Goldstein and Irving S. Reed

April 1996

Signal and Image Processing Institute
UNIVERSITY OF SOUTHERN CALIFORNIA
Department of Electrical Engineering-Systems
3740 McClintock Avenue, Room 400
Los Angeles, CA 90089-2564 U.S.A.

Theory of Partially Adaptive Radar

J. SCOTT GOLDSTEIN, Senior Member, IEEE
IRVING S. REED, Fellow, IEEE
University of Southern California

This work extends the recently introduced cross-spectral metric for subspace selection and dimensionality reduction to partially adaptive space-time sensor array processing. A general methodology is developed for the analysis of reduced-dimension detection tests with known and unknown covariance. It is demonstrated that the cross-spectral metric results in a low-dimensional detector which provides nearly optimal performance when the noise covariance is known. It is also shown that this metric allows the dimensionality of the detector to be reduced below the dimension of the noise subspace eigenstructure without significant loss. This attribute provides robustness in the subspace selection process to achieve reduced-dimensional target detection. Finally, it is demonstrated that the cross-spectral subspace reduced-dimension detector can outperform the full-dimension detector when the noise covariance is unknown, closely approximating the performance of the matched filter.

Manuscript received April 22, 1996; revised September 15 and November 16, 1996.

IEEE Log No. T-AES/33/4/06853.

This research was sponsored in part by DARPA and the USAF Rome Laboratory (AFMC) under Contract F30602-95-1-0001, the Army Research Laboratory under Contract DAAL01-96-P-0771 and a research grant by the Okawa Foundation.

Authors' address: Dept. of Electrical Engineering, EEB 528, University of Southern California, Los Angeles, CA 90089-2565; J. S. Goldstein is also with USAF Rome Laboratory, RL/C3BA, 525 Brooks Rd., Rome, NY 13441-4505.

I. INTRODUCTION

This work is concerned with optimal space-time adaptive processing (STAP) in environments which cannot support fully adaptive processing due to size, weight, and power restrictions. Typical sensor platforms which exhibit such restrictions include those that operate in airborne, space-segment, and undersea environments. The primary difficulty in STAP is that the dimension of the adaptive weight vector, which equals the product of the number of antenna elements and the number of Doppler bins, becomes large. Both the required sample support for STAP detection and the computational complexity of the algorithms, which update this weight vector, increase in proportion to the dimension of the weight vector. When the data from auxillary range gates are used for interference and clutter estimates, the required large sample support necessitates the use of range gates which are relatively far from the range gate of interest. These distant range gates may not preserve the homogeneity of the clutter and may not provide good estimates of the interference near the range gate of interest, thereby resulting in degraded performance.

Thus, real-time STAP implementations need a lower dimensional processor to be realizable from a computational viewpoint. A dilemma is encountered when the steady-state solution requires a larger number of weights than the platform can support. In this work a general methodology is developed which reduces the dimension of the weight vector for target detection without adversely affecting the steady-state solution.

The optimal weight vector for adaptive signal detection takes the form of a linearly constrained Wiener filter [1–7] where the constraint is in angle and Doppler. It is noted that this linear constraint for STAP detection is not the same as the popular minimum-variance, distortionless-response (MVDR) constraint for wideband arrays [8]. At first glance the form of the constrained Wiener filter for STAP and target detection does not provide much insight to the problem of reducing the dimension of the weight vector. As a consequence there is no clear methodology for finding the conditions needed to optimize a partially adaptive STAP system.

The most effective previously proposed reduced-rank solutions to the STAP problem require an eigendecomposition of the array covariance matrix or its estimate [9–15]. These methods are based on the principal component approximation of a covariance matrix [16, 17]. One goal of approximating the covariance matrix with a low-rank estimate is to simplify the weight update algorithm. Notably, the weight vector obtained by reducing the rank of the covariance matrix through these techniques has full dimension [12–15]. Finally, the principal component approach requires that the dimension of

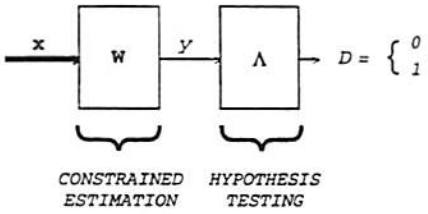

Fig. 1. Optimal joint Gaussian detector.

the noise subspace eigenstructure be known precisely. This dimension corresponds to the true rank of the interference-plus-clutter covariance matrix. Since this rank is never known a priori, it must be estimated. The penalty for underestimating the rank of this total noise contribution can be great; the detection performance degrades rapidly as the number of principal eigenvectors retained is decreased below the dimension of the noise subspace eigenstructure.

In this work a new method is introduced to achieve a reduced-dimension array processor using, what is called, a cross-spectral metric. The technique utilized here not only reduces the rank of the covariance matrix, but reduces the dimensionality of the problem itself. The largest eigenvalue magnitude criteria may also be used in the context of this new method for reduced-dimension detection, and the results are identical to that previously reported for the reduced-rank detection techniques.

The cross-spectral metric was introduced recently for narrowband MVDR processors and least-squares adaptive filters [18, 19]. For these cases the cross-spectral metric was shown to provide an upper-bound on the minimum mean-square error performance obtainable by all other eigen-based techniques.

Here the use of the cross-spectral metric is extended to STAP for target detection. It is shown that this metric also maximizes the output signal-to-interference plus noise ratio (SINR) [6, 20], thereby optimizing the weight vector for signal detection under the joint Gaussian assumption [3].

The optimal processor for detection under the joint Gaussian assumption is interpreted as consisting of two systems in cascade, as depicted in Fig. 1. The first system is a noise field estimator which utilizes the constrained Wiener filter. This estimation system produces the best estimate of the test cell with which the presence or absence of a target is to be determined. The second system consists of a hypothesis testing mechanism which implements the detection criterion. The input to the optimal processor is the observed radar return, and the output is a decision D with respect to target presence ($D = 1$) or absence ($D = 0$). With this interpretation of the optimal detector, the process of partial adaptivity belongs within the first system, and results in reduced-dimensional estimation.

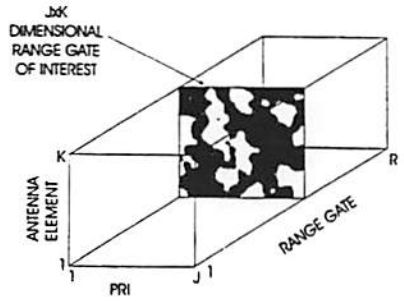

Fig. 2. 3-D CPI data cube.

The STAP detection criterion of primary interest in this work, termed an adaptive matched filter (AMF) constant false-alarm rate (CFAR) test, is reviewed with a known covariance in terms of the standard direct-form detector in Section II. The equivalent full-dimensional generalized sidelobe canceller (GSC) form [2, 21] of the detector is derived in Section III. The GSC form processor is utilized next in Section IV to derive a new reduced-dimensional GSC AMF CFAR detector which uses the cross-spectral metric. Here it is demonstrated that the cross-spectral metric maximizes the output SINR as a function of the dimension of the processor. The statistics of the reduced-dimension AMF CFAR test with known and unknown covariance are derived in Section V. An example of the performance of partially adaptive STAP for target detection is presented in Section VI. Extensions and the conclusions are provided in Section VII.

II. SPACE-TIME ADAPTIVE PROCESSING AND THE AMF CFAR TEST WITH KNOWN COVARIANCE

Radar returns are collected in a coherent processing interval (CPI), which can be represented as the 3-D data cube shown in Fig. 2. The data is then processed at one range of interest, which corresponds to a slice of the CPI data cube. This slice is a $J \times K$ space-time snapshot whose individual elements correspond to the data from the jth pulse repetition interval (PRI) and the kth sensor element [3, 22]. Hence this 2-D space-time data structure consists of element space information and PRI space-Doppler information. The snapshot is then stacked column-wise to form the $KJ \times 1$ vector $\mathbf{x}$.

If a target is present in the range gate of interest, then the return is composed of components due to the target, the interference sources or jammers, clutter, and white noise:

$$\mathbf{x} = \mathbf{x}_t + \mathbf{x}_i + \mathbf{x}_c + \mathbf{x}_w. \tag{1}$$

If no target is present, then the snapshot consists only of interference, clutter, and white noise. The total input noise vector $\mathbf{n}$ is given by

$$\mathbf{n} = \mathbf{x}_i + \mathbf{x}_c + \mathbf{x}_w. \tag{2}$$

The input noise covariance matrix is then defined to be

$$\mathbf{R} = \mathbf{E}[\mathbf{n}\mathbf{n}^H]. \tag{3}$$

Radar detection is a binary hypothesis problem, where hypothesis H_1 corresponds to target presence and hypothesis H_0 corresponds to target absence. Each of the components of the space-time snapshot vector $\mathbf{x}$ are assumed to be independent, complex, multivariate Gaussian. This snapshot, for each of the two hypothesis, is of the form,

$$\begin{aligned} H_0 &: \mathbf{x} = \mathbf{n} \\ H_1 &: \mathbf{x} = \mathbf{x}_t + \mathbf{n}. \end{aligned} \tag{4}$$

The $KJ \times 1$-dimensional space-time steering vector $\mathbf{v}(\vartheta_t, \omega_t)$ is defined as follows:

$$\mathbf{v}(\vartheta_t, \omega_t) = \mathbf{b}(\omega_t) \otimes \mathbf{a}(\vartheta_t) \tag{5}$$

where $\mathbf{b}(\omega_t)$ is the $J \times 1$ temporal steering vector at the target Doppler frequency ω_t and $\mathbf{a}(\vartheta_t)$ is the $K \times 1$ spatial steering vector in the direction provided by the target spatial frequency ϑ_t. The notation $(\cdot) \otimes (\cdot)$ represents the Kronecker tensor product operator. For convenience in the analysis to follow, the normalized steering vector in the space-time look-direction is defined to be

$$\mathbf{s} = \frac{\mathbf{v}(\vartheta_t, \omega_t)}{\sqrt{\mathbf{v}^H(\vartheta_t, \omega_t)\mathbf{v}(\vartheta_t, \omega_t)}}. \tag{6}$$

The two hypothesis in (4) may now be written in the form

$$\begin{aligned} H_0 &: \mathbf{x} = \mathbf{n} \\ H_1 &: \mathbf{x} = \alpha\mathbf{s} + \mathbf{n} \end{aligned} \tag{7}$$

where $\alpha = |\alpha|e^{j\phi}$ is a complex gain whose random phase ϕ is uniformly distributed between 0 and 2π. The random vector $\mathbf{x}$, when conditioned on ϕ, is Gaussian under both hypotheses. The conditional probability densities of $\mathbf{x}$ are

$$\begin{aligned} f_{x|H_1,\phi}(\mathbf{x}) &= \frac{1}{\pi^{KJ}\|\mathbf{R}\|} e^{-(\mathbf{x}-\alpha\mathbf{s})^H \mathbf{R}^{-1}(\mathbf{x}-\alpha\mathbf{s})} \\ f_{x|H_0,\phi}(\mathbf{x}) &= \frac{1}{\pi^{KJ}\|\mathbf{R}\|} e^{-\mathbf{x}^H \mathbf{R}^{-1}\mathbf{x}} \end{aligned} \tag{8}$$

where $\|(\cdot)\|$ is the determinant operator. The likelihood ratio test then takes the form,

$$\Lambda = \frac{f_{x|H_1}(\mathbf{x})}{f_{x|H_0}(\mathbf{x})} = \frac{\frac{1}{2\pi}\int_0^{2\pi} f_{x|H_1,\phi}(\mathbf{x})\,d\phi}{\frac{1}{2\pi}\int_0^{2\pi} f_{x|H_0,\phi}(\mathbf{x})\,d\phi} \underset{H_0}{\overset{H_1}{\gtrless}} \eta \tag{9}$$

where η is some threshold. Using the densities in (8), the test in (9) becomes

$$\Lambda = \mathbf{I}_0(2|\alpha|\,|\mathbf{s}^H\mathbf{R}^{-1}\mathbf{x}|)e^{-|\alpha|^2\mathbf{s}^H\mathbf{R}^{-1}\mathbf{s}} \underset{H_0}{\overset{H_1}{\gtrless}} \eta \tag{10}$$

where $\mathbf{I}_0(\cdot)$ is the modified Bessel function of the first kind. The noise covariance matrix $\mathbf{R}$ is nonnegative definite and the modified Bessel function is monotonically increasing in its argument. Therefore, the test in (10) reduces to

$$\Lambda_1 = |\mathbf{s}^H\mathbf{R}^{-1}\mathbf{x}|^2 \underset{H_0}{\overset{H_1}{\gtrless}} \eta_1 \tag{11}$$

where the new threshold η_1 is related to the previous threshold η as follows:

$$\eta_1 = \left[\frac{\mathbf{I}_0^{-1}(\eta e^{|\alpha|^2\mathbf{s}^H\mathbf{R}^{-1}\mathbf{s}})}{2|\alpha|}\right]^2. \tag{12}$$

The test in (11) was the first STAP detection criterion, developed in the well-known papers by Brennan and Reed [3] and Reed, Mallett, and Brennan (RMB) [4]. The RMB test takes the form of a matched filter for incoherent detection and is a Bayes optimal test which is maximally invariant with respect to the group of phase shifts. However, as noted by Kelly [23], no predetermined threshold can be set to achieve a specified false alarm probability since the detector is designed to operate in an unknown interference environment.

The RMB test in (11) can be modified to have a CFAR property via a normalization by the output power. This new AMF CFAR test, derived independently in [24] and [25], takes the form,

$$\Lambda_2 = \frac{|\mathbf{s}^H\mathbf{R}^{-1}\mathbf{x}|^2}{\mathbf{s}^H\mathbf{R}^{-1}\mathbf{s}} \underset{H_0}{\overset{H_1}{\gtrless}} \eta_2 \tag{13}$$

and is an optimum group invariant hypothesis test with respect to the change-of-scale and the initial target phase groups. The probability of detection for the AMF CFAR test Λ_2 is given by [24]

$$P_D = \sum_{n=0}^{\infty}\left(\frac{\xi^n e^{-\xi}}{n!}\right) Q(n+1, \eta_2) \tag{14}$$

where ξ is the output SINR, $Q(\cdot)$ is the incomplete gamma function, and the threshold η_2 is found from the false alarm probability:

$$P_{FA} = Q(1, \eta_2) = e^{-\eta_2}. \tag{15}$$

The RMB and AMF CFAR tests may be interpreted as functions of an optimal weight vector $\mathbf{w}_{\text{SINR}}$ [4], which is obtained by an unconstrained optimization of the SINR as follows:

$$\mathbf{w}_{\text{SINR}} = k\mathbf{R}^{-1}\mathbf{s} \tag{16}$$

where k is some arbitrary complex constant. The constrained optimization implemented by the sidelobe canceller form, which is introduced in the next section, fixes the value of k to provide a normalization by the output power. The weight vector in (16) is now

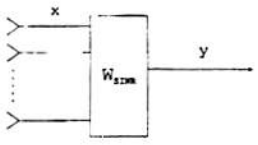

Fig. 3. Direct-form processor.

considered using a constrained optimization for target detection under the joint Gaussian assumption. The optimal constrained weight vector for maximizing the output SINR, while maintaining a normalized response in the target spatio-Doppler look-direction, was originally given in [2] as follows:

$$\mathbf{w}_{\text{SINR}} = \frac{\mathbf{R}^{-1}\mathbf{s}}{\mathbf{s}^H\mathbf{R}^{-1}\mathbf{s}}. \tag{17}$$

The output y formed by applying this latter weight vector to the primary data is

$$y = \mathbf{w}_{\text{SINR}}^H\mathbf{x} = \frac{\mathbf{s}^H\mathbf{R}^{-1}\mathbf{x}}{\mathbf{s}^H\mathbf{R}^{-1}\mathbf{s}} \tag{18}$$

and the resulting output SINR is

$$\xi = \frac{|\alpha|^2}{P} = \frac{|\alpha|^2}{\mathbf{w}_{\text{SINR}}^H\mathbf{R}\mathbf{w}_{\text{SINR}}} = |\alpha|^2\mathbf{s}^H\mathbf{R}^{-1}\mathbf{s} \tag{19}$$

where $|\alpha|^2$ is the output power due to the target signal under hypothesis H_1 and

$$P = \frac{1}{\mathbf{s}^H\mathbf{R}^{-1}\mathbf{s}} \tag{20}$$

is the output noise power of the processor. The weight vector in (17) is the result of a constrained optimization in which a beam is placed in that spatial and Doppler look-direction which is given by the steering vector s. This direct-form processor is depicted in Fig. 3.

The RMB test in (11) may now be expressed in the form

$$\Lambda_1 = (\mathbf{s}^H\mathbf{R}^{-1}\mathbf{s})^2|y|^2 = \left|\frac{y}{P}\right|^2 \underset{H_0}{\overset{H_1}{\gtrless}} \eta_1 \tag{21}$$

which demonstrates that the RMB detector compares a threshold η_1 with the ratio of the output power to the square of the noise output power. The normalized AMF test in (13) may similarly be written in the form,

$$\Lambda_2 = (\mathbf{s}^H\mathbf{R}^{-1}\mathbf{s})|y|^2 = \frac{|y|^2}{P} \underset{H_0}{\overset{H_1}{\gtrless}} \eta_2 \tag{22}$$

where the threshold η_2 is now compared with the ratio of the output power to the noise output power.

An equivalent new AMF CFAR detector is now developed which is characterized by a sidelobe canceller form. This sidelobe canceller form is used next to reduce the dimension of the weight vector $\mathbf{w}_{\text{SINR}}$, which maximizes the output SINR and the probability of detection under the joint Gaussian assumption. The goal of this data reduction step is to obtain a reduced-dimension test criterion which yields decisions which correspond with the full-dimension AMF CFAR test in (13).

III. GSC FORM PROCESSOR

The direct-form STAP processor described in Section II is transformed into the GSC form. The GSC processor results in an unconstrained weight vector and reformulates the STAP detector structure into the form of a standard Wiener filter. This GSC form of the detector provides a deeper insight to the rank-reduction and dimensionality reduction problems than appears to be possible otherwise.

Consider now using a unitary $KJ \times KJ$ matrix operator $\mathbf{T}$ to transform the data prior to detection. The resulting output SINR after such a transformation is identical to the original direct-form detection processor. The structure of this operator is partitioned as follows:

$$\mathbf{T} = \begin{bmatrix} \mathbf{s}^H \\ \mathbf{B} \end{bmatrix} \tag{23}$$

where the $KJ \times 1$-dimensional conventional space-time beamformer s is defined in (6) and $\mathbf{B}$ is the full-row rank $N \times KJ$ signal blocking matrix which maps $\mathbf{x}$ onto the null-space of s, where $N = (KJ - 1)$. Hence,

$$\mathbf{Bs} = \mathbf{0} \tag{24}$$

so that the matrix $\mathbf{B}$ effectively blocks any signal coming from the spatio-Doppler look direction. Any full row-rank matrix $\mathbf{B}$ that satisfies (24) and results in an invertible $\mathbf{T}$ is a valid signal blocking matrix. The Gram–Schmidt algorithm may be applied then to this matrix to generate an orthonormal $\mathbf{B}$ and a unitary $\mathbf{T}$. Two algorithms for directly finding an orthonormal $\mathbf{B}$, using the singular value decomposition (SVD) and the QR decomposition, respectively, are described in the Appendix.

The transformation of the radar return $\mathbf{x}$ by the operator $\mathbf{T}$ in (23) yields a vector $\tilde{\mathbf{x}}$ which has the form

$$\tilde{\mathbf{x}} = \mathbf{Tx} = \begin{bmatrix} \mathbf{s}^H\mathbf{x} \\ \mathbf{Bx} \end{bmatrix} = \begin{bmatrix} d \\ \mathbf{b} \end{bmatrix} \tag{25}$$

where the scalar-valued beamformed output is denoted by d. Here also the N-dimensional vector $\mathbf{b}$ is termed the noise subspace data vector. It is seen now that the transformed data vector $\tilde{\mathbf{x}}$ has an associated covariance matrix $\mathbf{R}_{\tilde{x}}$ which takes the form:

$$\mathbf{R}_{\tilde{x}} = \mathbf{TRT}^H = \begin{bmatrix} \sigma_d^2 & \mathbf{r}_{bd}^H \\ \mathbf{r}_{bd} & \mathbf{R}_b \end{bmatrix}. \tag{26}$$

The $N \times N$ noise subspace covariance matrix $\mathbf{R}_b$ is expressed by

$$\mathbf{R}_b = \mathbf{E}[\mathbf{bb}^H] = \mathbf{BRB}^H. \tag{27}$$

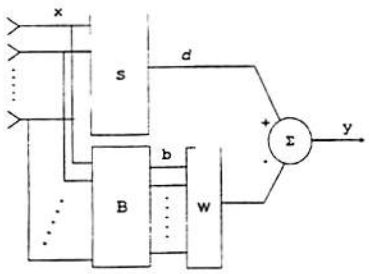

Fig. 4. Full-dimension GSC processor.

The $N \times 1$ cross-correlation vector between the noise subspace data vector and the beamformer output is given by

$$\mathbf{r}_{bd} = \mathbf{E}[\mathbf{b}d^*] = \mathbf{BRs} \tag{28}$$

where $*$ represents the complex conjugate operator. The scalar σ_d^2 in (26) is computed to be

$$\sigma_d^2 = \mathbf{s}^H\mathbf{Rs} \tag{29}$$

and represents the variance of the conventional beamformer output.

Next let $\mathbf{T}$ operate on the steering vector $\mathbf{s}$. This operation yields the unit transformed, steering vector $\mathbf{e}_1$, given by

$$\mathbf{e}_1 = \mathbf{Ts} = \begin{bmatrix} 1 \\ 0 \\ \vdots \\ 0 \end{bmatrix}. \tag{30}$$

Then the optimal weight vector in these transformed coordinates is given by

$$\mathbf{w}_{\text{gsc}} = \frac{\mathbf{R}_{\tilde{x}}^{-1}\mathbf{e}_1}{\mathbf{e}_1^H\mathbf{R}_{\tilde{x}}^{-1}\mathbf{e}_1} = \begin{bmatrix} 1 \\ -\mathbf{w} \end{bmatrix} \tag{31}$$

where $\mathbf{R}_{\tilde{x}}$ is the covariance matrix in (26). The partitioning of the matrix operator $\mathbf{T}$ leads naturally to the form of the GSC array processor depicted in Fig. 4 [2, 7, 21]. This processor results in a fixed weight of unity for the upper branch and an adaptive weight vector $\mathbf{w}$ of dimension $N = KJ - 1$ in the lower branch. The optimal value of the vector $\mathbf{w}$ in (31) is provided by the Wiener solution corresponding to the filter depicted in Fig. 4:

$$\mathbf{w} = \mathbf{R}_b^{-1}\mathbf{r}_{bd} \tag{32}$$

where $\mathbf{R}_b$ and $\mathbf{r}_{bd}$ are computed in (27) and (28), respectively. The GSC form processor implements the KJ-dimensional weight vector in (31) using the partitioning defined in (25). In a data adaptive mode of operation, the steady-state performance of the GSC and the direct-form processor are identical, but the adaptive weight vector $\mathbf{w}$ in the GSC is of a lower dimension. Hence, the computational requirements for updating this weight vector are reduced and the GSC form therefore can be considered canonical.

The output of the arrays, utilizing the weight vectors described in (17) and (31), are identical and, using (25) and (31), may be expressed as follows:

$$y = \mathbf{w}_{\text{SINR}}^H\mathbf{x} = \mathbf{w}_{\text{gsc}}^H\tilde{\mathbf{x}} = (\mathbf{s}^H - \mathbf{w}^H\mathbf{B})\mathbf{x}. \tag{33}$$

The output noise power is found by a substitution of (32) into (33) and the evaluation of the mean-square value of y using (20) as follows:

$$P = \frac{1}{\mathbf{s}^H\mathbf{R}^{-1}\mathbf{s}} = \sigma_d^2 - \mathbf{r}_{bd}^H\mathbf{R}_b^{-1}\mathbf{r}_{bd}. \tag{34}$$

The definitions of the filters $\mathbf{s}$ and $\mathbf{B}$ imply that the output SINR may be written by (19) in a more illuminating form as follows:

$$\xi = \frac{|\alpha|^2}{\sigma_d^2 - \mathbf{r}_{bd}^H\mathbf{R}_b^{-1}\mathbf{r}_{bd}}. \tag{35}$$

The observation data covariance matrix $\mathbf{R}_b$ is expressed now in terms of its eigenvectors and eigenvalues as follows:

$$\mathbf{R}_b = \mathbf{U}\Lambda\mathbf{U}^H \tag{36}$$

where $\mathbf{U}$ is a unitary $N \times N$ matrix composed of the eigenvectors $\{\mathcal{V}_i\}_{i=1}^N$ and Λ is the diagonal matrix of associated eigenvalues $\{\lambda_i\}_{i=1}^N$. The noise process $\mathbf{b}$, defined implicitly in (25) is transformed to a principal coordinate process $\mathbf{p}$ as follows:

$$\mathbf{p} = \mathbf{U}^H\mathbf{b}. \tag{37}$$

A normal component covariance matrix $\mathbf{R}_p$, cross-correlation vector $\mathbf{r}_{pd}$, and Wiener filter $\mathbf{w}_N$ are defined now as follows:

$$\mathbf{R}_p = \mathbf{E}[\mathbf{p}\mathbf{p}^H] = \mathbf{U}^H\mathbf{R}_b\mathbf{U} = \Lambda \tag{38}$$

$$\mathbf{r}_{pd} = \mathbf{E}[\mathbf{p}d^*] = \mathbf{U}^H\mathbf{r}_{bd} \tag{39}$$

$$\mathbf{w}_N = \mathbf{R}_p^{-1}\mathbf{r}_{pd} = \mathbf{U}^H\mathbf{w}. \tag{40}$$

The GSC in these normal coordinates, depicted in Fig. 5, is equivalent to the GSC in Fig. 4. In a data adaptive mode of operation, these two array processors have identical steady-state characteristics but may exhibit different transient behavior. The array output of the GSC in normal coordinates is given by

$$y = (\mathbf{s}^H - \mathbf{w}_N^H\mathbf{U}^H\mathbf{B})\mathbf{x} = (\mathbf{s}^H - \mathbf{w}^H\mathbf{B})\mathbf{x}. \tag{41}$$

Note that the output noise power,

$$P = \sigma_d^2 - \mathbf{r}_{pd}^H\mathbf{R}_p^{-1}\mathbf{r}_{pd} = \sigma_d^2 - \mathbf{r}_{bd}^H\mathbf{R}_b^{-1}\mathbf{r}_{bd} \tag{42}$$

and that the SINR,

$$\xi = \frac{|\alpha|^2}{\sigma_d^2 - \mathbf{r}_{pd}^H\mathbf{R}_p^{-1}\mathbf{r}_{pd}} = \frac{|\alpha|^2}{\sigma_d^2 - \mathbf{r}_{bd}^H\mathbf{R}_b^{-1}\mathbf{r}_{bd}} \tag{43}$$

are conserved by the operator $\mathbf{U}$.

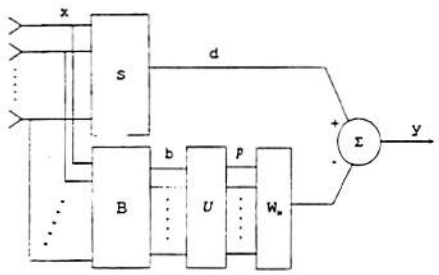

Fig. 5. Full-dimension GSC processor in principal coordinates.

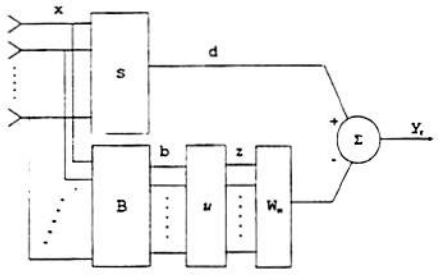

Fig. 6. Reduced-dimension GSC processor.

IV. PARTIALLY ADAPTIVE STAP AND THE CROSS-SPECTRAL METRIC

We now derive the cross-spectral metric for optimal subspace selection and dimensionality reduction in partially adaptive STAP. The problem of reducing the degrees of freedom for an array processor involves selecting a subset or some combination of the elements to be adaptively weighted. For notational purposes, let the space spanned by the columns of the fully adaptive array covariance matrix be denoted by $\mathcal{C}^N$, implying that the observation covariance matrices $\mathbf{R}_b$ and $\mathbf{R}_p$ are of dimension $N \times N$ and the vectors $\mathbf{r}_{bd}$, $\mathbf{r}_{pd}$, $\mathbf{w}$, and $\mathbf{w}_N$ are $N \times 1$-dimensional vectors. The partially adaptive GSC shown in Fig. 6 utilizes an $N \times M$ transformation operator $\mathcal{U}$, in place of $\mathbf{U}$ in Fig. 5, to form the order M reduced-dimension observation data vector,

$$\mathbf{z} = \mathcal{U}^H \mathbf{b} \tag{44}$$

where $M < N$. The associated $M \times M$ reduced-dimension covariance matrix is given by

$$\mathbf{R}_z = \mathcal{U}^H \mathbf{R}_b \mathcal{U} = \Lambda_M \tag{45}$$

where Λ_M is the diagonal matrix composed of the M eigenvalues corresponding to the eigenvectors to be selected which form $\mathcal{U}$. The cross-correlation between the process $\mathbf{z}$ and the beamformed signal d is given by

$$\mathbf{r}_{zd} = \mathbf{E}[\mathbf{z}d^*] = \mathcal{U}^H \mathbf{r}_{bd}. \tag{46}$$

The data vector $\mathbf{z}$ is then processed by the reduced-dimension weight vector $\mathbf{w}_M$, which is of dimension $M \times 1$. From Wiener filter theory this weight vector is expressed finally by

$$\mathbf{w}_M = \mathbf{R}_z^{-1} \mathbf{r}_{zd} = \Lambda_M^{-1} \mathcal{U}^H \mathbf{r}_{bd}. \tag{47}$$

The most popular technique for subspace selection is based on the principal components method [9–15]. This method determines the SVD of the $N \times N$-dimensional covariance matrix $\mathbf{R}_b$ and selects the M largest eigenvectors (those corresponding to the largest eigenvalues) to form the M-dimensional eigen-subspace $\Psi \subset \mathcal{C}^N$ in which the adaptive processor operates. However, this technique does not directly consider the maximum output SINR performance measure to maximize the probability of detection, which is a function of not only the space spanned by the noise covariance matrix $\mathbf{R}_b$ but also of the cross-correlation between the beamformed signal d and the noise process $\mathbf{b}$.

The derivation in [18] is now used to reduce the dimension of the Wiener filter in a manner which maximizes the output SINR. To accomplish this consider the selection of an $N \times M$ transformation matrix $\mathcal{U}$, which is composed of some M columns from $\mathbf{U}$ (see Fig. 6). The operator $\mathcal{U}$ is constrained therefore to be a subset of M of the N possible eigenvectors of $\mathbf{R}_b$. This particular constraint allows a direct comparison with the principal component technique, which chooses the dimensionality reducing transform $\mathcal{U}$ to be composed of those M eigenvectors which correspond to the largest M eigenvalues. Thus, the particular problem at hand is to choose the subspace spanned by a set of M eigenvectors out of the N available such that the resulting M-dimensional Wiener filter yields the largest output SINR out of all $\binom{N}{M}$ possible combinations of eigenvectors. The subspace spanned by the columns of the optimal reduced-dimensional covariance matrix which achieves this maximization of the output SINR as a function of filter dimension is denoted by $\Omega \subset \mathcal{C}^N$.

Now denote the reduced-dimensional processor output by y_r. This is illustrated in Fig. 6. A study of Figs. 5 and 6 suggest that the reduced-dimensional processor output may be expressed by the relation,

$$y_r = [1, \quad \mathbf{w}_N^H \mathbf{U}^H - \mathbf{w}_M^H \mathcal{U}^H] \begin{bmatrix} y \\ \mathbf{b} \end{bmatrix}. \tag{48}$$

Denote the weight error vector between the full-dimension weight vector and its reduced-dimension version by

$$\varepsilon = \mathbf{U}\mathbf{w}_N - \mathcal{U}\mathbf{w}_M. \tag{49}$$

By (42) the output noise power for the reduced-dimension processor is now computed in this notation to be

$$P_r = \sigma_d^2 - \mathbf{r}_{pd}^H \mathbf{R}_p^{-1} \mathbf{r}_{pd} + \varepsilon^H \mathbf{R}_b \varepsilon \geq P \tag{50}$$

and the SINR of the reduced-dimension processor is expressed as

$$\xi_r = \frac{|\alpha|^2}{\sigma_d^2 - \mathbf{r}_{pd} \mathbf{R}_p^{-1} \mathbf{r}_{pd} + \varepsilon^H \mathbf{R}_b \varepsilon} \leq \xi. \tag{51}$$

Note that the target signal power is not affected by reducing the dimension of the problem; the reduction in dimensionality is only a function of the noise field estimation. A comparison of (42) with (50) or (43) with (51), shows that it is desirable to choose the dimensionality reducing operator $\mathcal{U}$ in a manner that minimizes the additional mean-square error. Define the $N \times M$ subspace index matrix $\mathbf{J}$, given by

$$\mathbf{J} = \mathbf{U}^H \mathcal{U}. \tag{52}$$

This matrix is composed of N orthonormal unit vectors and N-M null vectors in an order which corresponds with the selection of the M columns of $\mathbf{U}$ that were retained to form the dimensionality reducing operator $\mathcal{U}$. Now, one wants to minimize the scalar term $\varepsilon^H \mathbf{R}_b \varepsilon$ which appears in (50) and (51) as follows:

$$\min[\varepsilon^H \mathbf{R}_b \varepsilon] = \min[(\mathbf{w}_N^H \mathbf{R}_p^{1/2} - \mathbf{w}_M^H \mathbf{R}_z^{1/2} \mathbf{J}^H) \times (\mathbf{R}_p^{1/2} \mathbf{w}_N - \mathbf{J}\mathbf{R}_z^{1/2} \mathbf{w}_M)]. \tag{53}$$

Thus evidently the best solution for (53) is to choose that set of M rows of $\mathbf{U}$ for the $M \times N$ matrix $\mathcal{U}$ such that $\mathbf{J}\mathbf{R}_z^{1/2}\mathbf{w}_M$ is the best low dimensional approximation to the vector $\mathbf{R}_p^{1/2}\mathbf{w}_N$.

The Wiener–Hopf relationship for the full-dimensional case is given by

$$\mathbf{R}_p \mathbf{w}_N = \mathbf{r}_{pd}. \tag{54}$$

A multiplication of both sides of (54) by $\mathbf{R}_p^{-1/2}$ on the left yields the following relationships:

$$\mathbf{R}_p^{1/2}\mathbf{w}_N = \mathbf{R}_p^{-1/2}\mathbf{r}_{pd} = \mathbf{\Lambda}^{-1/2}\mathbf{U}^H\mathbf{r}_{bd} = \begin{bmatrix} \frac{\mathcal{V}_1^H \mathbf{r}_{bd}}{\sqrt{\lambda_1}} \\ \frac{\mathcal{V}_2^H \mathbf{r}_{bd}}{\sqrt{\lambda_2}} \\ \vdots \\ \frac{\mathcal{V}_N^H \mathbf{r}_{bd}}{\sqrt{\lambda_N}} \end{bmatrix} \tag{55}$$

where $\mathbf{U}$ is the unitary matrix composed of the eigenvectors $\{\mathcal{V}_i\}_{i=1}^N$ and $\mathbf{\Lambda}$ is the diagonal matrix of associated eigenvalues $\{\lambda_i\}_{i=1}^N$. Hence in order to make the vector $\mathbf{J}\mathbf{R}_z^{1/2}\mathbf{w}_M$ be the best low dimensional approximation to the vector $\mathbf{R}_p^{1/2}\mathbf{w}_N$, it is necessary to rank order the terms in (55) by their magnitude. With this ranking of the eigenvectors which compose the matrix $\mathbf{U}$, the index matrix $\mathbf{J}$ takes the form

$$\mathbf{J} = \begin{bmatrix} \mathbf{I} \\ \mathbf{0} \end{bmatrix} \tag{56}$$

where $\mathbf{I}$ is the $M \times M$ identity matrix and 0 is the $(N - M) \times M$ null matrix. Then the dimensionality reducing operator $\mathcal{U}$ is selected by choosing those M eigenvectors of $\mathbf{U}$ which correspond with the largest M values of the sequence of non-negative terms

$$\left| \frac{\mathcal{V}_i^H \mathbf{r}_{bd}}{\sqrt{\lambda_i}} \right|^2 \tag{57}$$

for $i = 1,2,\ldots N$. Note that the metric in (57) measures the cross-spectral energy projected along the ith eigenvector. With this selection, the columns of the reduced-dimensional covariance matrix $\mathbf{R}_z$ span the M dimensional cross-spectral subspace $\Omega \subset \mathcal{C}^N$ to provide the largest output SINR of any M dimensional subspace which is spanned by M of the N columns of $\mathbf{U}$.

Clearly, the subspace Ω spanned by the columns of eigenvectors corresponding with the M largest values of the cross-spectral metric is not the same as the subspace Ψ spanned by the eigenvectors corresponding with the M largest eigenvalues for all values of M. This means that the Wiener filter in the cross-spectral subspace Ω yields an output SINR which is always larger than or equal to that provided by the Wiener filter in the subspace Ψ. We conclude that the reduced-dimension Wiener filter found via the cross-spectral metric maximizes the output SINR as a function of the order of the filter for the eigenvector basis. Thus the cross-spectral metric results in an upper-bound on the performance of eigen-based rank and dimensionality reduction techniques.

To demonstrate that the cross-spectral metric is optimal for each filter order $M \leq N$, we consider the decomposition of the SINR performed by the full-dimensional matrix of eigenvectors $\mathbf{U}$. The output SINR of the full-dimension processor, from (38) and (43), can be expressed as

$$\xi = \frac{|\alpha|^2}{\sigma_d^2 - \sum_{i=1}^N \frac{|\mathcal{V}_i^H \mathbf{r}_{bd}|^2}{\lambda_i}}. \tag{58}$$

The optimal SINR of the reduced-dimension processor is expressed as

$$\xi_r = \frac{|\alpha|^2}{\sigma_d^2 - \sum_{j \in \Omega} \frac{|\mathcal{V}_j^H \mathbf{r}_{bd}|^2}{\lambda_j}}. \tag{59}$$

Finally, a comparison of the decision rule in (57) with the expressions in (58) and (59) demonstrate that the cross-spectral metric maximizes the output SINR as a function of the order of the weight vector.

V. REDUCED-DIMENSION AMF CFAR TEST WITH KNOWN AND UNKNOWN CONVARIANCE

The AMF CFAR test in (13) is defined in terms of the output signal y and the output noise power P of the direct-form processor. The GSC is then derived as

the canonical form of this optimal array processor in Section III, where it is also demonstrated that the GSC yields an output signal and SINR which are equivalent with that provided by the direct-form processor.

An optimal reduced-dimensional STAP design technique is derived in Section IV, where the GSC form processor is utilized. It is also shown in Section IV that the target signal power is not affected by a reduction of the weight vector dimensionality. Thus, as mentioned in Section I, the process of dimensionality reduction for partially adaptive STAP belongs within the noise field estimation system shown in Fig. 1. The cross-spectral metric provides an upper-bound on the output SINR achievable by reduced-rank and reduced-dimension detectors using an eigenvector basis. This fact explains why the cross-spectral metric provides the capability to achieve a reduction in the dimensionality of the weight vector below the dimension of the noise subspace eigenstructure without a significant loss in performance. The cross-spectral metric given in (57) provides the best set of the possible $\binom{N}{M}$ eigenvectors of the noise subspace covariance matrix to select for dimensionality reduction. These optimal eigenvectors are then used by the hypothesis testing mechanism to determine target presence or absence. A new optimal reduced-dimensionality AMF CFAR test is now formally defined and analyzed.

A. Reduced-Dimension AMF CFAR Test with Known Covariance

For convenience, we now rewrite the AMF CFAR test in (22) as follows:

$$\Lambda_2 = \frac{|\mathbf{s}^H\mathbf{R}^{-1}\mathbf{x}|^2}{\mathbf{s}^H\mathbf{R}^{-1}\mathbf{s}} = \frac{|y|^2}{P} \underset{H_0}{\overset{H_1}{\gtrless}} \eta_2. \tag{60}$$

The array output of the reduced-dimension processor y_r, derived in (48) and depicted in Fig. 6, is written now in the form,

$$y_r = (\mathbf{s}^H - \mathbf{w}_M^H\mathcal{U}^H\mathbf{B})\mathbf{x} = d - \mathbf{w}_M^H\mathbf{z} = d - \mathbf{r}_{zd}^H\mathbf{R}_z^{-1}\mathbf{z}. \tag{61}$$

Also the output noise power of the reduced-dimension processor P_r in (50) may be expressed by

$$P_r = \sigma_d^2 - \mathbf{r}_{zd}^H\mathbf{R}_z^{-1}\mathbf{r}_{zd} \tag{62}$$

where the covariance matrix $\mathbf{R}_z$ and the cross-correlation vector $\mathbf{r}_{zd}$ were defined in (45) and (46), respectively. In terms of the expressions in (61) and (62), a new optimal reduced-dimension version of the AMF CFAR test is obtained as follows:

$$\Lambda_{2_r} = \frac{|y_r|^2}{P_r} \underset{H_0}{\overset{H_1}{\gtrless}} \eta_2 \tag{63}$$

where the SINR of the reduced-dimension processor is given by

$$\xi_r = \frac{|\alpha|^2}{\sigma_d^2 - \mathbf{r}_{zd}\mathbf{R}_z^{-1}\mathbf{r}_{zd}}. \tag{64}$$

The probability of detection of this new reduced-dimension AMF CFAR test in (63) is now given by

$$P_{D_r} = \sum_{n=0}^{\infty}\left(\frac{(\xi_r)^n e^{-\xi_r}}{n!}\right) Q(n+1,\eta_2) \tag{65}$$

which is similar in form to (14), and the probability of false alarm retains the form in (15):

$$P_{FA} = Q(1,\eta_2) = e^{-\eta_2}. \tag{66}$$

Note that the expressions in (61)–(66) are valid for any unitary operator used for dimensionality reduction with a subspace selection rule which chooses M of the N columns of the unitary operator. This includes, but is not limited to the reduced-dimension principal component and cross-spectral AMF CFAR tests, which use the unitary matrix composed of the eigenvectors of $\mathbf{R}_b$.

B. Reduced-Dimension AMF CFAR Test with Unknown Covariance

The reduced-dimension AMF CFAR test is now examined for the case of unknown covariance. The standard approach for radar detection when the noise covariance is unknown is to obtain an estimate from some $L > KJ$ range gates in the neighborhood of the range gate currently being tested for signal presence. The data in the range gate of interest is termed the primary data. The L nearby range gates, which yield what is termed the secondary or auxillary data, are assumed to be target free. It is also possible to assume that only multiple snapshots of the same range gate are available. The presentation of the material in this section follows similar derivations given previously for full-dimension detectors [24–30].

It is well known that the maximum likelihood estimate of the covariance matrix $\mathbf{R}$ is provided by the sample covariance matrix $\hat{\mathbf{R}}$, i.e.,

$$\hat{\mathbf{R}} = \frac{1}{L}\sum_{i=1}^{L}\mathbf{n}_i\mathbf{n}_i^H \tag{67}$$

where $\mathbf{n}_i$ is the $KJ \times 1$ vector of samples from the ith nearby range gate. Define an auxillary $KJ \times L$ data matrix $\mathbf{A}$ by

$$\mathbf{A} = [\mathbf{n}_1, \quad \mathbf{n}_2 \quad \ldots \quad \mathbf{n}_L] \tag{68}$$

so that the sample covariance matrix $\hat{\mathbf{R}}$ may be written in the form,

$$\hat{\mathbf{R}} = \frac{1}{L}\mathbf{A}\mathbf{A}^H. \tag{69}$$

Then the AMF CFAR test is expressed in terms of the sample covariance matrix as follows:

$$\Lambda_{2_s} = \frac{|\mathbf{s}^H\hat{\mathbf{R}}^{-1}\mathbf{x}|^2}{\mathbf{s}^H\hat{\mathbf{R}}^{-1}\mathbf{s}} = \frac{L|\mathbf{s}^H(\mathbf{A}\mathbf{A}^H)^{-1}\mathbf{x}|^2}{\mathbf{s}^H(\mathbf{A}\mathbf{A}^H)^{-1}\mathbf{s}} \underset{H_0}{\overset{H_1}{\gtrless}} \eta_2. \quad (70)$$

The data matrix $\mathbf{A}$ is expressed now in the form

$$\mathbf{A} = \mathbf{R}^{1/2}\mathbf{X} \quad (71)$$

where $\mathbf{X}$ is a $KJ \times L$ matrix of zero-mean, independent and identically distributed, complex Gaussian variates with unit variance. Then an equivalent test to the sampled data AMF CFAR test in (70) is provided by

$$\Lambda_{2_s} = \frac{L|\mathbf{s}^H\mathbf{R}^{-1/2}(\mathbf{X}\mathbf{X}^H)^{-1}\mathbf{R}^{-1/2}\mathbf{x}|^2}{\mathbf{s}^H\mathbf{R}^{-1/2}(\mathbf{X}\mathbf{X}^H)^{-1}\mathbf{R}^{-1/2}\mathbf{s}} \underset{H_0}{\overset{H_1}{\gtrless}} \eta_2. \quad (72)$$

The methodology used in the previous section for transforming the observed data into the GSC form is now applied to the auxillary data. The new normalized transformed steering vector is given by

$$\mathbf{v} = \frac{\mathbf{R}^{-1/2}\mathbf{s}}{\sqrt{\mathbf{s}^H\mathbf{R}^{-1}\mathbf{s}}} \quad (73)$$

and the unitary matrix $\mathbf{T}$ in (23) is redefined to be

$$\mathbf{T} = \begin{bmatrix} \mathbf{v}^H \\ \mathbf{B}_v \end{bmatrix} \quad (74)$$

where $\mathbf{B}_v = \text{null}(\mathbf{v})$ is the $N \times KJ$ blocking matrix associated with the vector $\mathbf{v}$ (which can be found using one of the methods presented in the Appendix), $\mathbf{T}\mathbf{v} = \mathbf{e}_1$, the vector $\mathbf{e}_1$ is defined in (30), and $N = KJ - 1$. The matrix $\mathbf{T}$ operates on the data matrix $\mathbf{X}$ defined in (71). The transformed data matrix $\tilde{\mathbf{X}}$ has the form,

$$\tilde{\mathbf{X}} = \mathbf{T}\mathbf{X} = \begin{bmatrix} \mathcal{D} \\ \mathcal{B} \end{bmatrix} \quad (75)$$

where $\mathcal{D}$ is the $1 \times L$ beamformed data vector and $\mathcal{B}$ is the $N \times L$ noise subspace data matrix.

The dimensionality reducing $N \times M$ transform $\mathcal{U}$, defined to be composed of those M eigenvectors of $\mathcal{B}\mathcal{B}^H$ which maximize the cross-spectral metric given in (57) with $\mathbf{r}_{bd} = \mathbf{B}_v\mathbf{X}\mathbf{X}^H\mathbf{v}$, is applied next to form a $(M+1) \times (M+1)$ transformed reduced-dimensional sample covariance matrix as follows:

$$\hat{\mathbf{R}}_{\tilde{X}} = \begin{bmatrix} 1 & \mathbf{0}^H \\ \mathbf{0} & \mathcal{U}^H \end{bmatrix} \mathbf{T}\mathbf{X}\mathbf{X}^H\mathbf{T}^H \begin{bmatrix} 1 & \mathbf{0}^H \\ \mathbf{0} & \mathcal{U}^H \end{bmatrix}^H$$

$$= \begin{bmatrix} \mathcal{D}\mathcal{D}^H & \mathcal{D}\mathcal{Z}^H \\ \mathcal{Z}\mathcal{D}^H & \mathcal{Z}\mathcal{Z}^H \end{bmatrix} = \begin{bmatrix} \hat{\sigma}_d^2 & \hat{\mathbf{r}}_{zd}^H \\ \hat{\mathbf{r}}_{zd} & \hat{\mathbf{R}}_z \end{bmatrix} \quad (76)$$

where the reduced-dimensional $M \times L$ auxillary data vector $\mathcal{Z}$ is given by

$$\mathcal{Z} = \mathcal{U}^H\mathcal{B}. \quad (77)$$

The primary data is also transformed by $\mathbf{R}^{-1/2}$ and $\mathbf{T}$ to obtain

$$\mathbf{x}_p = \mathbf{T}\mathbf{R}^{-1/2}\mathbf{x} = \begin{bmatrix} d \\ \mathbf{b} \end{bmatrix} \quad (78)$$

and the reduced-dimension $M \times 1$ primary data vector is then given by

$$\mathbf{z}_p = \mathcal{U}^H\mathbf{b}. \quad (79)$$

The optimal $(M+1) \times 1$-dimensional weight vector in these transformed coordinates is given by

$$\hat{\mathbf{w}}_{\text{gsc}} = \begin{bmatrix} 1 \\ -\hat{\mathbf{w}}_r \end{bmatrix} \quad (80)$$

where the $M \times 1$-dimensional vector $\hat{\mathbf{w}}_r$ is provided by the Wiener solution corresponding to the filter depicted in Fig. 4, namely

$$\hat{\mathbf{w}}_r = (\mathcal{Z}\mathcal{Z}^H)^{-1}\mathcal{Z}\mathcal{D}^H = \hat{\mathbf{R}}_z^{-1}\hat{\mathbf{r}}_{zd}. \quad (81)$$

The resulting output power is given by

$$\hat{P}_r = \hat{\sigma}_d^2 - \hat{\mathbf{r}}_{zd}^H\hat{\mathbf{R}}_z^{-1}\hat{\mathbf{r}}_{zd}. \quad (82)$$

The reduced-dimension AMF CFAR test with an unknown covariance corresponding to the test in (70) is expressed now in the form,

$$\Lambda_{2_{sr}} = \frac{|d - \hat{\mathbf{w}}_r^H\mathbf{z}_p|^2}{\hat{\sigma}_d^2 - \hat{\mathbf{r}}_{zd}^H\hat{\mathbf{R}}_z^{-1}\hat{\mathbf{r}}_{zd}} = \frac{|y_r|^2}{\hat{P}_r} \underset{H_0}{\overset{H_1}{\gtrless}} \eta_{2_s} \quad (83)$$

where the threshold η_{2_s} in (83) is related to the original threshold η_2 in (70) by

$$\eta_{2_s} = \frac{\eta_2}{L}. \quad (84)$$

Next the denominator of the reduced-dimension sampled data AMF CFAR test in (83) is rewritten in the form,

$$\hat{P}_r = \mathcal{D}(\mathbf{I} - \mathcal{Z}^H\hat{\mathbf{R}}_z^{-1}\mathcal{Z})\mathcal{D}^H = \mathcal{D}\mathbf{C}\mathcal{D}^H. \quad (85)$$

The vector $\mathcal{D}$ is a $1 \times L$ zero-mean, white Gaussian random vector. Therefore the distribution of $\mathcal{D}$ can be denoted by

$$\mathcal{D} \longleftrightarrow N_L(\mathbf{0}, \mathbf{I}) \quad (86)$$

where $N_L(\mathbf{0}, \mathbf{I})$ is a joint Gaussian density of zero mean and covariance $\mathbf{I}$, the $L \times L$ identity matrix. Also it is easily shown by (77) that the matrix $\mathbf{I} - \mathbf{C}$, given by

$$(\mathbf{I} - \mathbf{C}) = \mathcal{Z}^H\hat{\mathbf{R}}_z^{-1}\mathcal{Z} \quad (87)$$

is a projection matrix of rank M which projects vectors onto the reduced-dimension auxillary data noise subspace. The matrix $\mathbf{C}$ is also an idempotent projection matrix of rank $L - M$, and the distribution of $\hat{P}_r$ is therefore central χ^2 with $L - M$ degrees of freedom [31]. Thus the distribution of $\hat{P}_r$ is expressed by

$$\hat{P}_r \longleftrightarrow \chi^2_{L-M}. \quad (88)$$

The output of the reduced-dimension GSC form array variate may be expressed next by

$$y_r = d - \hat{\mathbf{r}}_{zd}^H \hat{\mathbf{R}}_z^{-1} \mathbf{z}_p \tag{89}$$

which is conditionally complex Gaussian distributed when the quantities $\mathbf{z}_p$ and $\mathcal{Z}$ are fixed. The conditional covariance of y_r is ρ^{-1}, where

$$\rho = \frac{1}{1 + \mathbf{z}_p^H \hat{\mathbf{R}}_z^{-1} \mathbf{z}_p}. \tag{90}$$

The parameter ρ is the well-known RMB loss factor [4, 25, 27, 32] for the reduced-dimension processor, and it has a central Beta distribution which is given by

$$f_\rho(\rho) = \frac{\rho^{L-M}(1-\rho)^{M-1}}{\beta(M, L-M+1)} \tag{91}$$

where

$$\beta(a,b) = \frac{(a-1)!(b-1)!}{(a+b-1)!}. \tag{92}$$

Hence the distribution of the reduced-dimension AMF CFAR test is given by

$$\Lambda_{2_{sr}}(y_r, \hat{P}_{n_r} | \mathbf{z}_p, \mathcal{Z}) \longleftrightarrow \rho^{-1} \frac{\chi^2(\delta)}{\chi^2_{L-M}} = \frac{\gamma}{\rho} \tag{93}$$

where δ is the noncentrality parameter, given by

$$\delta = \rho \xi_r. \tag{94}$$

The parameter γ is the ratio of two independent χ^2 variables where the numerator is noncentral χ^2 distributed. Hence, under hypothesis H_1, γ has a noncentral F distribution [31] given by

$$f_{\gamma|\rho,H_1}(\gamma) = \frac{e^{-\delta}}{\beta(1, L-M)(1+\gamma)^{L-M+1}} \times {}_1F_1\left(L-M+1, 1, \frac{\delta\gamma}{1+\gamma}\right). \tag{95}$$

Therefore, the conditional distribution of the test $\Lambda_{2_{sr}}$ given $\mathbf{z}_p$ and $\mathcal{Z}$ under hypothesis H_1, may be expressed by

$$f_{\Lambda_{2_{sr}}|\rho,H_1}(q) = \frac{e^{-\delta}}{\beta(1, L-M)} \frac{\rho}{(1+q\rho)^{L-M+1}} \times {}_1F_1\left(L-M+1, 1, \frac{\delta q\rho}{1+q\rho}\right). \tag{96}$$

The unconditional probability density function of the reduced-dimension AMF CFAR test is then computed as follows:

$$f_{\Lambda_{2_{sr}}|H_1}(q) = \int_0^1 f_{\Lambda_{2_{sr}}|\rho,H_1}(q) f_{\rho|H_1}(\rho)\, d\rho \tag{97}$$

which is expressible in the form,

$$f_{\Lambda_{2_{sr}}|H_1}(q) = \frac{1}{\beta(1, L-M)\beta(M, L-M+1)} \times \int_0^1 e^{-\delta} \frac{\rho^{L-M+1}(1-\rho)^{M-1}}{(1+q\rho)^{L-M+1}} \times {}_1F_1\left(L-M+1, 1, \frac{\delta q\rho}{1+q\rho}\right) d\rho \tag{98}$$

where $q \geq 0$. Finally by (98) for a fixed threshold η, the probability of detection is computed to be

$$\begin{aligned} P_D(\eta) &= \int_\eta^\infty f_{\Lambda_{2_{sr}}|H_1}(q)\, dq \\ &= \int_0^1 \frac{e^{-\delta}\rho^{L-M}(1-\rho)^{M-1}}{\beta(1, L-M)\beta(M, L-M+1)} \\ &\quad \times \int_{\eta\rho/1+\eta\rho}^1 (1-q)^{L-M-1} \\ &\quad \times {}_1F_1(L-M+1, 1, \delta q)\, dq\, d\rho \\ &= 1 - \frac{1}{\beta(M, L-M+1)} \int_0^1 e^{-\delta}\rho^{L-M}(1-\rho)^{M-1} \\ &\quad \times \sum_{k=0}^\infty \frac{\delta^k}{k!} \mathcal{I}\left(\frac{\eta\rho}{1+\eta\rho}, k+1, L-M\right) d\rho \end{aligned} \tag{99}$$

where $\mathcal{I}(x,a,b)$ is the incomplete beta function. The distribution of the reduced-dimension AMF CFAR test under hypothesis H_0 requires that the variable δ be set to zero, and (98) reduces to

$$f_{\Lambda_{2_{sr}}|H_0}(q) = \frac{1}{\beta(1, L-M)\beta(M, L-M+1)} \times \int_0^1 \frac{\rho^{L-M+1}(1-\rho)^{M-1}}{(1+q\rho)^{L-M+1}} d\rho \tag{100}$$

which, for the selected threshold η, yields a false alarm probability given by

$$\begin{aligned} P_{FA}(\eta) &= \int_\eta^\infty f_{\Lambda_{2_{sr}}|H_0}(q)\, dq \\ &= \frac{1}{\beta(1, L-M)\beta(M, L-M+1)} \\ &\quad \times \int_\eta^\infty \int_0^1 \frac{\rho^{L-M+1}(1-\rho)^{M-1}}{(1+q\rho)^{L-M+1}} d\rho\, dq \\ &= \frac{1}{\beta(M, L-M+1)} \int_0^1 \left(\frac{\rho}{1+\eta\rho}\right)^{L-M} \\ &\quad \times (1-\rho)^{M-1}\, d\rho. \end{aligned} \tag{101}$$

Since the P_{FA} is only a function of the threshold η and the integers L and M, all of which are held fixed, the test $\Lambda_{2_{sr}}$ is CFAR.

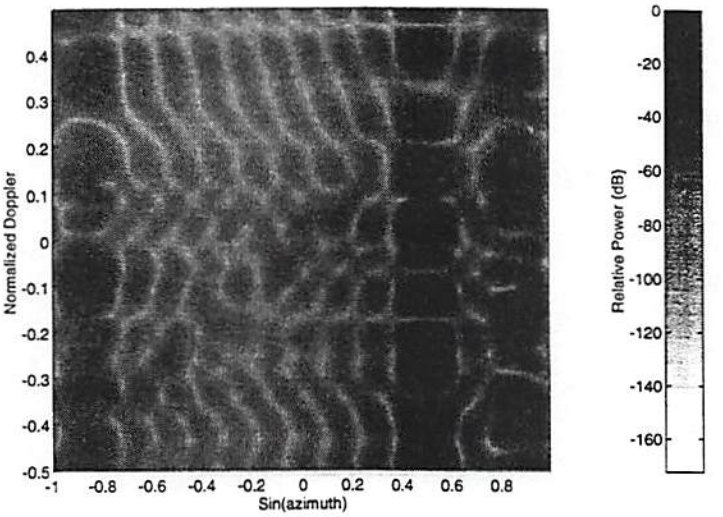

Fig. 7. Power spectrum of data.

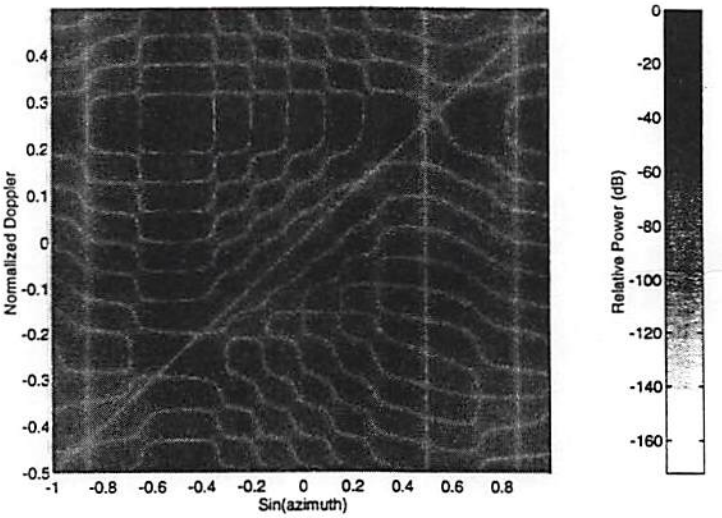

Fig. 8. Full-dimension optimal Wiener filter.

VI. AN EXAMPLE OF THE PERFORMANCE OF PARTIALLY ADAPTIVE RADAR

A simulation is now considered which utilizes the parameters of the DARPA Mountaintop radar in order to compare the performance of the reduced-dimension detectors with that of the full-dimension, joint domain optimal detector. The AMF CFAR test is utilized exclusively for this example.

The Mountaintop radar employs the Radar Surveillance Technology Experimental Radar (RSTER) and the Inverse Displaced Phase Center Array (IDPCA), both colocated at the same site [33]. It is assumed that the radar is in the RSTER-90 configuration and the receive-only mode. The transmit frequency is 450 MHz. This radar consists of $K = 14$ elements and $J = 16$ pulses in the PRI. The elevation angle θ is fixed (pre-beamformed), and the azimuth angle ϕ is the only free parameter. The dimension of the adaptive processor is $KJ = 224$. The GSC processor beamforms the target signal in the top branch and utilizes in the lower branch a blocking matrix $\mathbf{B}$ which blocks the target signal from being observed at the weight vector. The noise subspace data vector in the lower branch is then of dimension $N = KJ - 1 = 223$. The corresponding full-dimension GSC weight vector is also of dimension 223×1.

For the purposes of this analysis, three barrage jammers and land clutter compose the interference enviroment. Also one target signal is assumed to be present. It is assumed that the radar platform is at a height of 500 m, and that the platform velocity is 500 m/s. The target, which is assumed also to be at a height of 500 m, has a range of 22 km and an azimuth of $-30°$. The target velocity is 250 m/s. This target has a signal-to-noise ratio (SNR) of 15 dB, representing a small, nonfluctuating, constant radar cross-section target. The three jammers have azimuth angles of $-60°$, $30°$, and $60°$, with jammer-to-noise ratios of 30 dB, 40 dB, and

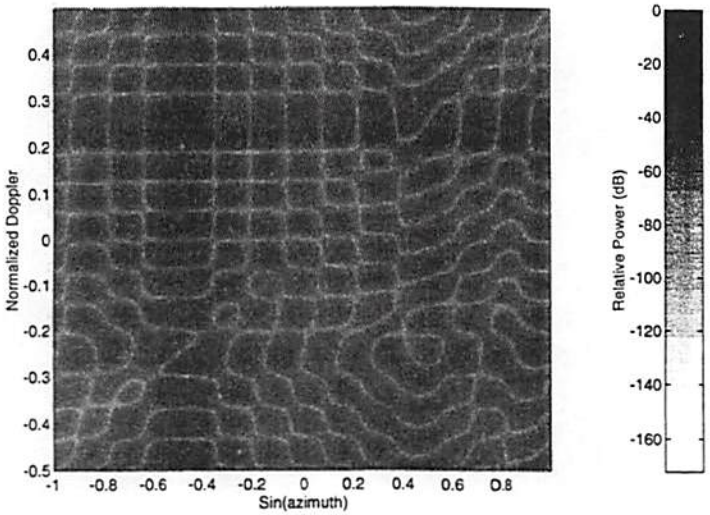

Fig. 9. Reduced-dimension eigen-subspace Wiener filter.

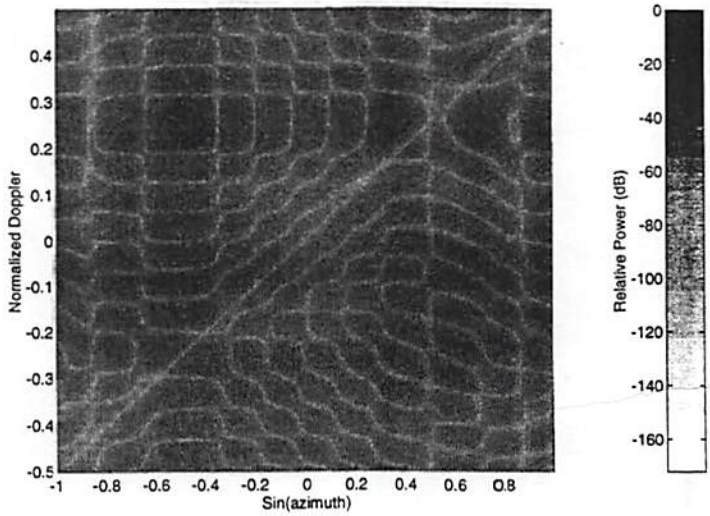

Fig. 10. Reduced-dimension cross-spectral subspace Wiener filter.

30 dB, respectively. The clutter-to-noise ratio is set to be 30 dB.

The cross-spectral metric is now applied to the GSC and the detection performance is compared with the principal component techniques such as PCI [14, 15] and the Eigencanceler [12, 13]. The performance of the fully adaptive GSC, the partially adaptive eigen-subspace GSC, and the partially adaptive cross-spectral subspace GSC processors are evaluated.

To obtain the performance of the subspace selection techniques, the dimension of the adaptive processor is assumed to be reduced from $N = 223$ weights to $M = 50$. The dimension of the noise subspace eigenstructure is calculated to be approximately 70. This is the lower bound needed for the standard rank or dimensionality reduction techniques [9–11].

The power spectrum of the data, averaged over 500 snapshots, is presented in Fig. 7, from which it is evident that the target signal is not discernible. Fig. 8 presents the gain of the optimal space-time Wiener filter, in which it is seen that this space-time weight vector of dimension 223 is capable of attenuating all jammers and clutter while simultaneously passing the target signal. The full-dimension Wiener filter yields an output SINR of 38.28 dB.

Fig. 9 depicts the space-time gain of the 50-dimensional eigen-subspace Wiener filter. The clutter and most of the power from the three jammers is passed with relatively high gain; there is little attenuation of the noise. The output SINR obtainable by the 50-dimensional eigen-subspace Wiener filter is 25.98 dB, reflecting a loss of 12.3 dB.

The space-time gain of the 50-dimensional cross-spectral subspace Wiener filter is depicted in Fig. 10. It can be seen that by simply selecting a different set of 50 eigenvectors, the resulting array response closely approximates the full-dimension optimal STAP matched filter and the clutter and jammers are attenuated. The resulting output SINR

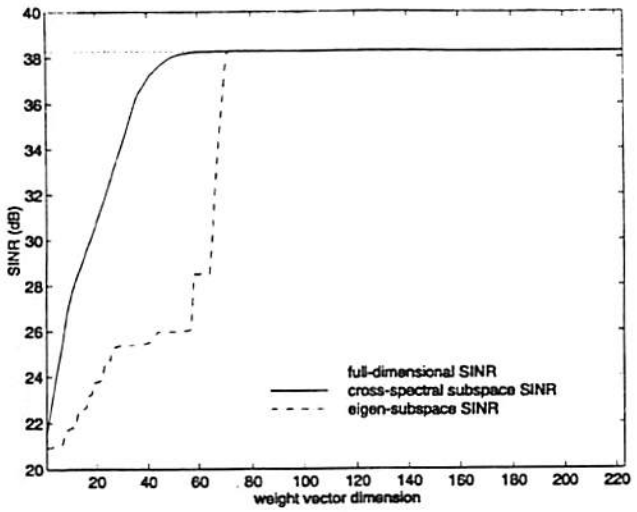

Fig. 11. Output SINR of reduced-dimension processors as function of Wiener filter order.

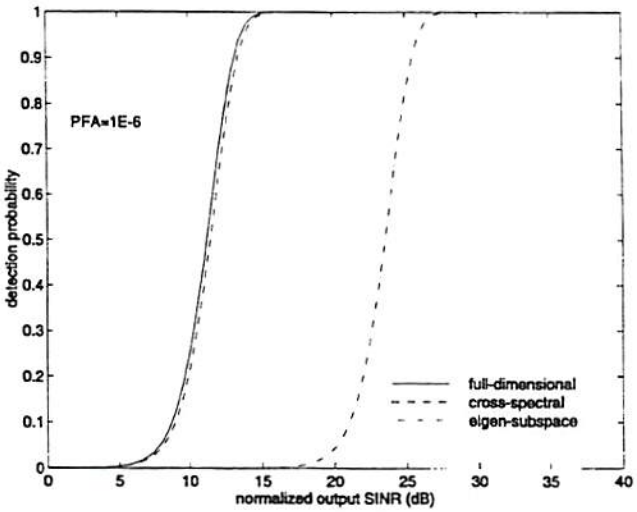

Fig. 12. AMF CFAR test probability of detection versus normalized output SINR for case of known covariance.

is 38.03 dB, reflecting a loss of only 0.25 dB in the reduction of the weight vector dimension from 223 to 50. This is due to the better selection of the 50 eigenvectors of $\mathbf{R}$ obtained by a use of the cross-spectral metric.

The performance of these two reduced-dimension processors may also be evaluated by plotting the output SINR as a function of Wiener filter order. The SINR for the eigen-subspace and cross-spectral subspace reduced-dimension processors are compared with the full-dimesnional SINR in Fig. 11 as the dimension increases from 1 to 223. It can be seen from this figure that the eigen-subspace processor converges to the optimal SINR in an abrupt manner, thereby obtaining the optimal value only when the Wiener filter order reaches the dimension of the noise subspace eigenstructure. This is characteristic of the eigen-subspace techniques in nearly all of its applications since the principal components method does not yield an optimal filter as a function of order. By contrast the cross-spectral metric depicts an exponential-like convergence to the optimal SINR.

The above simulation shows that the reduced-dimension Wiener filter in the cross-spectral subspace outperforms the Wiener filter in the eigen-subspace for all filter orders less than the dimension of the noise subspace eigenstructure. It is verified in Fig. 11 that the cross-spectral metric provides an upper-bound to the SINR performance achievable by a reduction of the number of eigenvectors of the array covariance matrix. Finally, note for the Mountaintop radar example that the reduction of the weight vector dimension to 50 weights can be interpreted as an error in the estimation of the dimension of the noise subspace eigenstructure. It is clear from Fig. 11 that the penalty in SINR performance for underestimating the rank of the noise subspace eigenstructure is greatly reduced in the cross-spectral approach to dimensionality reduction. This robustness property is paramount for reduced-dimension detection of targets in unknown noise environments.

Next the probability of a false alarm for each test is set to $P_{FA} = 10^{-6}$. The detection probabilities with known noise covariance are calculated for the full-dimension test (223 adaptive weights) and for the two reduced-dimension tests (50 adaptive weights) in the eigen-subspace and the cross-spectral subspace. The resulting plots of P_D versus the normalized output SINR are presented in Fig. 12. The normalized SINR is calculated by dividing the output SINR of each reduced-dimension detector by the output SINR of the full-dimension detector. It is seen that the full-dimension AMF CFAR detector and the 50-dimensional cross-spectral AMF CFAR detector exhibit very similar performance. By comparison the 50-dimensional eigen-subspace detector performs quite poorly. Recall that a target input SNR of 15 dB is used in the graphical examples presented earlier in this section. The full-dimension and cross-spectral AMF CFAR detectors both yield a detection probability which is nearly equal to unity for this target. The eigen-subspace detector, however, yields a P_D which is near zero for this same scenario. The 50-dimensional cross-spectral subspace detector yields a 12 dB improvement in detection sensitivity over the 50-dimensional eigen-subspace detector. This corresponds with the estimated 12 dB gain of the cross-spectral subspace processor over the SINR obtainable by the eigen-subspace processor depicted in Fig. 11.

The performance of the AMF CFAR detector with unknown covariance is now considered. The false alarm probability is evaluated as a function of the threshold while the dimension of the detector, which is N for the full-dimension and M for the

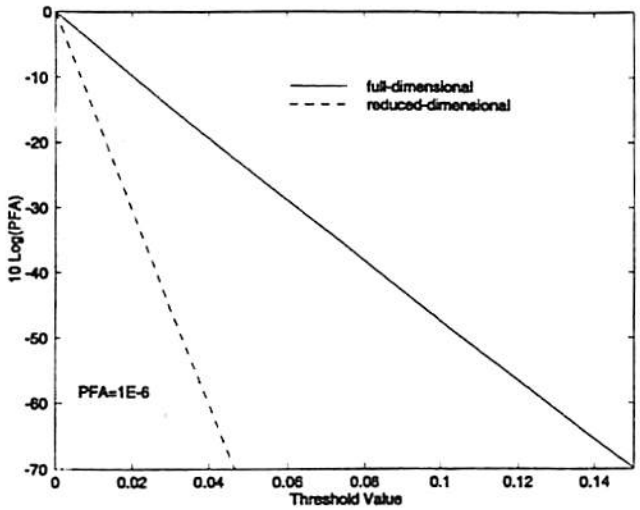

Fig. 13. False alarm probability as function of threshold for full-dimension and reduced-dimension detectors.

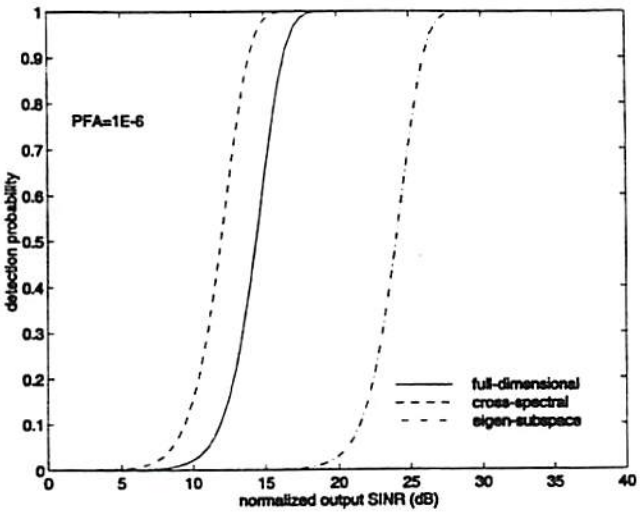

Fig. 14. AMF CFAR test probability of detection versus normalized output SINR for case of unknown covariance.

reduced-dimension, and the number of range gates used to estimate the covariance, which is $L = 2KJ = 448$, are held fixed. The graph in Fig. 13 demonstrates that in order to obtain $P_{FA} = 10^{-6}$, the full-dimension detector ($N = 223$) must select the threshold to be $\eta = 0.1270$, and the reduced-dimension detectors ($M = 50$) must utilize a threshold which is set to be $\eta = 0.0390$. Next, these required values for the threshold are used along with the output SINR, which is calculated for the Mountaintop radar example above, in order to determine the performance of the full-dimension and reduced-dimension AMF CFAR detectors. The probability of detection versus the normalized output SINR is depicted in Fig. 14 for the case when the noise covariance is unknown.

The full-dimension AMF CFAR test performs approximately 3 dB below the case when the covariance is known. Also the 50-dimensional eigen-subspace AMF CFAR detector with an unknown and estimated covariance performs approximately 10 dB below that of the full-dimension AMF CFAR detector with unknown covariance. When the covariance is known, this reduced-dimension detector performs 12 dB below the full-dimension detector due to the SINR loss. This SINR loss between the full-dimension and eigen-subspace detector is partially offset by the fact that the threshold for the reduced-dimension detectors is lower than the threshold for the full-dimension case. A comparison of the detection sensitivity for the eigen-subspace AMF CFAR detector with known and unknown covariances demonstrates that the latter case is degraded by only approximately 0.5 dB.

Conversely, the 50-dimensional cross-spectral subspace detector outperforms the full-dimension AMF CFAR detector. Here it is shown that the subspace selection by the cross-spectral metric provides an output SINR which is nearly equivalent to that of the full-dimension case. However by lowering the threshold for this reduced-dimension detector, the detection probability calculation integrates over a broader range of values thereby yielding a 2.5 dB increase in detection sensitivity as compared with the full-dimension detector when the noise covariance is unknown. It is noted that the detection performance of the cross-spectral subspace AMF CFAR test with unknown covariance is only 0.5 dB less than the full-dimension AMF CFAR test with known covariance (the matched filter).

VII. CONCLUSIONS

A general methodology is introduced in this paper to describe reduced-dimension detectors and to analyze their statistical properties and performance. In particular, closed form expressions are derived for the detection and false alarm probabilities under the conditions of both known and unknown covariance matrices. Although the AMF CFAR test is emphasized in this paper, the analysis techniques developed herein extend readily to nearly any other test simply by relating the variables which compose the test to the GSC.

The computational complexity requirements of the eigendecomposition performed for subspace selection suggest that other procedures need to be discussed. It is noted that other unitary operators $\mathbf{U}$ may be used with the cross-spectral metric to determine the transformation $\mathcal{U}$, to yield new reduced-dimension tests which may exhibit approximately the optimal performance obtained herein. The Gram–Schmidt procedure introduced by Brennan and Reed [34–36] is one method for achieving a lower complexity transformation to find the cross-spectral metric. Another example is to approximate the cross-spectral metric with a unitary operator which does not completely decorrelate the noise subspace covariance

[18] Goldstein, J. S., and Reed, I. S. (1997)
Subspace selection for partially adaptive sensor array processing.
IEEE Transactions on Aerospace Electronic Systems, **33**, 2 (Apr. 1997).

[19] Goldstein, J. S., and Reed, I. S. (1997)
Reduced rank adaptive filtering.
IEEE Transactions on Signal Processing, **45**, 2 (Feb. 1997).

[20] Goldstein, J. S., and Reed, I. S. (1997)
Performance measures for optimal constrained beamformers.
IEEE Transactions on Antennas Propagation, **45**, 1 (Jan. 1997).

[21] Griffiths, L. J., and Jim, C. W. (1982)
An alternative approach to linearly constrained adaptive beamforming.
IEEE Transactions on Antennas Propagation, **AP-30**, 1 (Jan. 1982), 27–34.

[22] Ward, J. (1994)
Space-time adaptive processing for airborne radar.
Technical report 1015, MIT Lincoln Laboratory, Dec. 1994.

[23] Kelly, E. J. (1986)
An adaptive detection algorithm.
IEEE Transactions on Aerospace and Electronic Systems, **AES-23** (Nov. 1986), 115–127.

[24] Chen, W. S., and Reed, I. S. (1991)
A new CFAR detection test for radar.
Digital Signal Processing, **4** (Oct. 1991), 198–214.

[25] Robey, F. C., Fuhrmann, D. R., Kelly, E. J., and Nitzberg, R. (1992)
A CFAR adaptive matched filter detector.
IEEE Transactions on Aerospace and Electronic Systems, **28**, 1 (Jan. 1992), 208–216.

[26] Kelly, E. J. (1985)
Adaptive detection in non-stationary interference, Part I and Part II.
Technical report TR-724, MIT Lincoln Laboratory, June 1985.

[27] Yu, X., and Reed, I. S. (1995)
Adaptive detection of signals with linear feature mappings and representations.
IEEE Transactions on Signal Processing, **43**, 12 (Dec. 1995), 2953–2963.

[28] Reed, I. S., Gau, Y. L., and Truong, T. K.
A simultaneous CFAR detection and ML estimation STAP algorithm for airborne radar.
IEEE Transactions on Aerospace and Electronic Systems, to be published.

[29] Monticciolo, P. (1994)
Adaptive detection in stationary and nonstationary noise environments.
Technical report TR-937, MIT Lincoln Laboratory, Feb. 1994.

[30] Steinhardt, A. (1992)
Adaptive multisensor detection and estimation.
In S. Haykin and A. Steinhardt (Eds.), *Adaptive Radar Detection and Estimation.*
New York: Wiley, 1992, ch. 3.

[31] Muirhead, R. J. (1982)
Aspects of Multivariate Statistical Theory.
New York: Wiley, 1982.

[32] Kelly, E. J. (1987)
Adaptive detection in non-stationary interference, Part III.
Technical report TR-761, MIT Lincoln Laboratory, Aug. 1987.

[33] Titi, G. W. (1994)
An overview of the ARPA/Navy Mountaintop Program.
In *Proceedings of the IEEE Adapt. Ant. Systems Symposium*, Long Island, NY, Nov. 1994.

[34] Brennan, L. E., Mallett, J. D., and Reed, I. S. (1977)
Convergence rate in adaptive arrays.
Technical report TSC-PD-A177-2, Technology Service Corporation, July 1977.

[35] Brennan, L. E., and Reed, I. S. (1978)
Convergence rate in adaptive arrays.
Technical report TSC-PD-A177-4, Technology Service Corporation, Jan. 1978.

[36] Monzingo, R. A., and Miller, T. W. (1980)
Introduction to Adaptive Arrays.
New York: Wiley, 1980.

[37] Strang, G. (1988)
Linear Algebra and its Applications.
San Diego, CA: Harcourt Brace Jovanovich, 1988.

[38] Golub, G. H., and Van Loan, C. F. (1990)
Matrix Computations.
Baltimore, MD: The John Hopkins University Press, 1990.

J. Scott Goldstein (S'86—M'88—SM'96) is a Ph.D. candidate in electrical engineering at the University of Southern California.

He is the Vice-President and Chief Scientist of Adaptronics, Inc. He is also a reserve officer in the U.S. Air Force, assigned as the Program Manager for MILSATCOM Systems and the Project Leader for Signal Processing Development at the USAF Rome Laboratory. Mr. Goldstein serves on the DARPA Steering Committee for Space-Time Adaptive Processing, and has been employed by the U.S. Army Research Laboratory as a consultant on image processing since 1994. From 1981 to 1990, he served in the U.S. Army, being branch qualified infantry and signal. From 1990 to 1992, he was associated with both the George Mason University Center of Excellence in C3I and the Institute for Defense Analyses. From 1992 to 1995, he was with the Radar Systems Division of the Sensors and Electromagnetic Applications Laboratory at the Georgia Tech Research Institute. His research interests include adaptive and statistical signal processing, detection and estimation theory, and image processing.

Mr. Goldstein is a member of Sigma Xi, Tau Beta Pi and Eta Kappa Nu. He has received the IEEE Aerospace and Electronic System Society's EASCON Award, the AFCEA Postgraduate Fellowship, and the 1996 Japanese Okawa Foundation Research Grant. In addition, he has received over 15 Air Force Awards for Scientific Achievement due to his research in radar and communications theory.

Irving S. Reed (SM'69—F'73) was born on Nov. 12, 1923 in Seattle, WA. He received the B.S. and Ph.D. degrees in mathematics from the California Institute of Technology in 1944 and 1949, respectively.

From 1951 to 1960, he was associated with Lincoln Laboratory, Massachusetts Institute of Technology. From 1960 to 1963, he was a Senior Staff Member with the RAND Corporation. Since 1963, he has been a Professor of Electrical Engineering and Computer Science at the University of Southern California, where he currently holds the Charles Lee Powell Chair. He is also a consultant to the RAND Corporation and is a Director of Adaptive Sensors, Inc. His research interests include mathematics, VLSI computer design, coding theory, stochastic processes, information theory, image processing, and statistical signal processing.

Dr. Reed is a member of the National Academy of Engineering. He has authored and coauthored approximately 300 publications, and is the holder of six U.S. patents. He has received fourteen NASA Awards for Outstanding Technical Contributions, the USC Associates Award for Creativity in Research and Scholarship, the IEEE Aerospace and Electronic Systems Society's M. Barry Carlton Memorial Award for Best Paper, the IEEE Richard W. Hamming Medal, and the Distinguished Alumni Award from the California Institute of Technology. Dr. Reed was a Shannon Lecturer at the IEEE International Symposium on Information Theory, and was presented with the IEEE Information Theory Society's Shannon Award in 1995. He also received the 1995 IEEE Masaru Ibuka Consumer Electronics Award.